Journal of Hazardous Materials 192 (2011) 704–713

Contents lists available at ScienceDirect

Journal of Hazardous Materials

journal homepage: www.elsevier.com/locate/jhazmat

# Discrimination of organic solid materials by LIBS using methods of correlation and normalized coordinates

R.J. Lasheras, C. Bello-Gálvez, E.M. Rodríguez-Celis [1], J. Anzano *

*Laser Laboratory and Environment, Department of Analytical Chemistry, Faculty of Sciences, University of Zaragoza, Pedro Cerbuna #12, 50009 Zaragoza, Spain*

ARTICLE INFO

*Article history:*
Received 18 February 2011
Received in revised form 20 May 2011
Accepted 23 May 2011
Available online 12 June 2011

*Keywords:*
LIBS
Identification
Organic solid materials
Spectral libraries

ABSTRACT

The methods of linear and rank correlation and normalized coordinates (MNC) have been applied to the identification of organic solid materials with a very similar chemical composition by laser-induced breakdown spectroscopy (LIBS). The present study evaluated these three statistical methods using an Echelle spectrometer coupled with an intensified charge-coupled device (ICCD). Moreover, three instrumental parameters (laser pulse energy, delay time and integration time) were evaluated in terms of their influence on the signal-to-noise ratio of carbon and hydrogen emission lines. The probability of a right identification can be estimated by means the described methods in this paper. Methods of correlation provide better identification and discrimination than normalized coordinates at a 95% confidence level.



## 1. Introduction

Laser-induced breakdown spectroscopy (LIBS), also known as laser-induced plasma spectroscopy (LIPS), is an elemental analysis technique with several fields of application [1]. One of them is the qualitative and quantitative analysis of samples with an unknown composition [2]. The main advantage of the LIBS-technique is that sample preparation is not necessary, moreover is almost non-destructive. However, matrix effects and poor accuracy are common in the quantitative analysis LIBS. Nowadays, the most widely employed lasers for LIBS are Nd:YAG lasers. In general, in the LIBS process, when the intense laser beam is focused onto the solid sample, a small volume of the target is heated in a very short time producing a plume of material above the surface where plasma is formed. The spectral composition of the light emitted by this plasma plume depends on the elemental composition of the sample, which is analyzed by a spectrometer. Although, limitations for identification exist due to the loss of molecular information in plasma, the technique achieves excellent potential for online, real-time analysis [3]. LIBS is basically an optical emission spectroscopy where the intensities of atomic lines of different species present in the sample under local thermodynamic equilibrium (LTE) are compared. If thermodynamic equilibrium exists, the relative populations of atomic energy levels are determined by the equilibrium temperature. LTE exists after a sufficient number of collisions have occurred to thermalize the plasma, and heavy species (atoms and ions) and light species (electrons) are in equilibrium [4].

Some variables that can influence LIBS measurements are laser related (i.e. wavelength, energy, pulse duration and shot-to-shot power fluctuation), focusing spot size, ambient conditions, physical properties of the sample, amplification detector gain, ambient atmosphere, pressure and the detection window (delay time, integration time gate) [5]. The optimization of LIBS methods is habitually performed by univariate procedures [6] and multivariate procedures can be used to construct a robust calibration model for LIBS spectra [7].

Conventional optimization through univariate methodology requires a great amount of experiments and is time consuming; moreover, interactions among variables are not evaluated. Another aspect is the fact that applying univariate procedures, it will be rarely possible to reach really optimized values. Multivariate techniques are alternative, economical and effective methods that allow the simultaneous optimization of more than one variable [8]. Univariate and multivariate calibration have been compared and both have showed a similar performance in accuracy and precision [9].

LIBS can be successfully applied for the identification of solid and particulate materials. Different statistical methods have been applied for compound identification using LIBS. Among them are correlation methods, such as linear or parametric correlation and rank or nonparametric correlation [10–12], ratios determination [13,14], principal component analysis (PCA) [15,16], partial least squares discriminant analysis (PLS-DA) [17], soft independent modelling of class analogy (SIMCA) [18], artificial neural networks (ANN) [19] and method of normalized coordinates (MNC) [20]. LIBS

* Corresponding author. Tel.: +34 976762684; fax: +34 976761292.
*E-mail address:* janzano@unizar.es (J. Anzano).
[1] When the work was done, she was affiliated with the Department of Chemistry at the University of Florida in Gainesville.

0304-3894/$ – see front matter © 2011 Elsevier B.V. All rights reserved.
doi:10.1016/j.jhazmat.2011.05.074

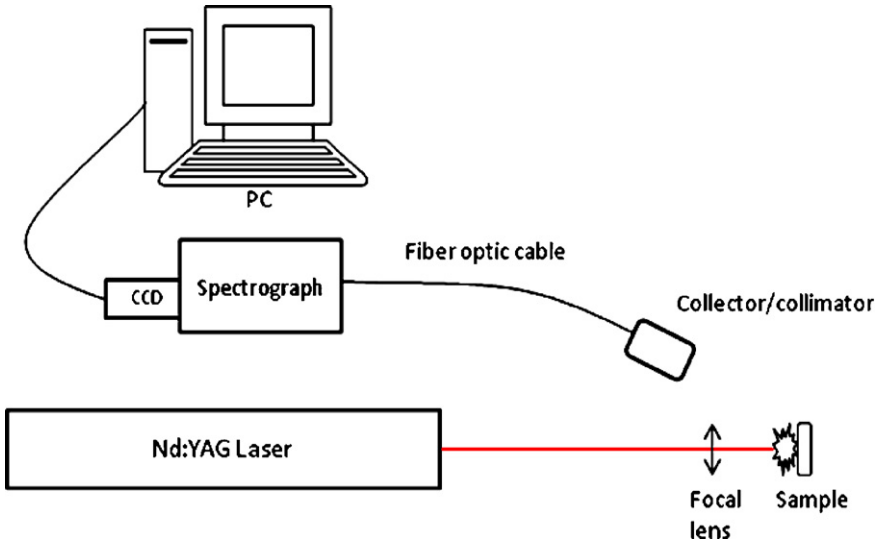


**Fig. 1.** Experimental set-up.

is used for identification of solid materials as soils [21], metal alloys [22], and archaeological materials [23], etc.

In the present work, LIBS parameters were optimized and a statistical study of a right identification of organic solid materials using as detector system an Echelle spectrometer coupled to an intensified coupled-charge device was done. The signal-to-noise ratio (SNR) was studied for parameters such as pulse energy, delay time and temporal integration time. Optimal parameters to identify organic solid materials were studied; therefore, the carbon (247.9 nm) and hydrogen (656.3 nm) emission lines were selected for this optimization. The spectra were smoothed for improving the SNR by means of the method of adjacent averaging. The laser energy was studied from 5 to 322 mJ. The delay time was monitored using an energy laser of 132 mJ for both elements. The laser-induced plasma plume was characterized at optimal conditions in order to verify the existence of LTE. The plasma temperature and density electron were determined.

For the identification of organic solid materials the spectrum of the "unknown" sample was compared with a spectra library. A reference spectra library LIBS was obtained for 11 organic solid materials: polystyrene (PS), polypropylene (PP), high- and low-density polyethylene (HDPE, LDPE), polyethylene terephthalate (PET), polyvinyl chloride (PVC), poly(tetrafluoroethene) (PTFE), poly(tetrafluoroethene) with 15% aluminium, nylon, cellulose and rubber. The spectra library is made of 165 spectra examined with three different approaches to identify organic solid materials. Several statistical techniques were used such as linear and rank correlation, and MNC. The efficiency of sample identification were investigated by means these statistical techniques. Two of these methods, linear and rank correlation have been applied successfully to identify solid materials [10], polymers [11,12], glasses [24] and paper materials for forensic purpose [25]. The method of normalized coordinates has been mostly used to identify polymers. This approach was described by Ferrero et al. [20] based on the algebraic determination of the problem spectrum coordinates with respect to the library base. Its most important advantage is that, unlike linear correlation, it allows detection of a mixture of several substances in a sample. It considers the presence of all elements in the library, and minimize any doubt in discrimination of false positives. Moreover, if a substance is absent in the library, this method will be able to identify it because its spectrum is compared with all the spectra in the library.

## 2. Experimental

### 2.1. Instrumental set-up

The LIBS set-up is shown in Fig. 1. The remaining instrumentation used consisted of a Nd:YAG laser, an *xyz*-type carrying stage for the sample (Standa 011957), a spectrograph and an intensified charged coupled device (ICCD) detector. A Nd:YAG laser (Brilliant Quantel, Q-Switched) with a 350 mJ laser pulse energy at 1064 nm, a 4.4 ns pulse duration and 0.7 Hz repetition frequency was used with a 90 mm focal length lens. Plasma light was collected and transported to a spectrograph by a lens and optical fiber (fused silica, 50 μm core diameter). An external collector/collimator was used as collected lens; its position was adjusted at 200 mm by a diode laser (Andor, HE-OPI-0009). An Echelle spectrograph (Andor Mechelle ME5000, 195 mm focal length, F/7, resolution of $\lambda/\Delta\lambda$ 5000, spectral range from 200 to 975 nm) was coupled to an ICCD detector (Andor iStar DH734, 1024′1024 pixels, 13.6′13.6 $\mu m^2$/pixel, 18 mm intensifying diameter and exposure time was 0.011 s). This system was calibrated by a Hg:Ar lamp (Ocean Optics, HG-1, Hg–Ar lines 253–922 nm). MCP gain was fixed at 200. The energy laser, gate delay and integration times were optimized depending on SNR.

### 2.2. Experimental procedure

Polymer samples from recycled materials of organic compounds were used. A small piece of plastic (approximately $3 \times 3$ cm) was placed on double-sided tape stuck to a glass slide. The piece of plastic must be completely stuck to the slide in order to avoid air between them. The experimental procedure of this study is shown in Fig. 2. It consisted of the following steps:

*Step* 1: Optimization of LIBS parameters (laser energy, delay and integration time) in order to obtain the best SNR. The SNR value was calculated as a correct signal/noise peak to peak (pk–pk) where corrected signal is equal to signal height/average noise, and noise (pk–pk) is defined as maximum noise/minimum noise. Firstly, for improving the SNR, all spectra were smoothed using the method of averaging adjacent for improving the SNR. The development of an informatic application as a part of the study of optimal parameters consisted on a simple program, which allowed to calculate the SNR for carbon and hydrogen emission lines, simultaneously, such SNR peak–peak as RMS.

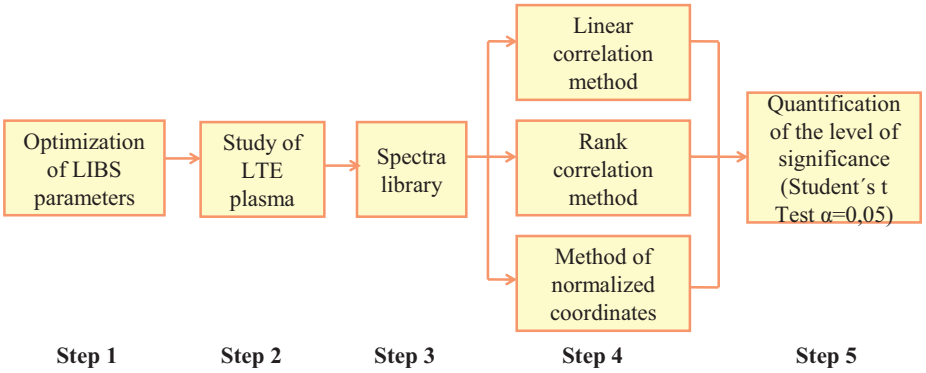


**Fig. 2.** Scheme of the experimental procedure.

The purpose was studied the optimal conditions to identify organic solid materials, therefore the carbon (247.9 nm) and hydrogen (656.3 nm) emission lines were selected. The laser energy was studied from 5 to 322 mJ at 1064 nm. The laser energy can be modified changing the parameter QS-delay from 195 (maximum energy) to 500 μs (minimum energy). A Gentec-EO SOLO-PE Laser Power & Energy Meter was used for finding out the relationship between QS-delay and pulse laser energy. The delay time was studied in the range from 100 to 10000 ns and the integration time from 500 to 25,000 ns.

*Step* 2: LTE plasma was studied on optimal conditions.

*Step* 3: One spectral library was built using the spectra of high- and low-density polyethylene, polypropylene, polystyrene, polyethylene terephthalate, poly-vinyl chloride, poly(tetrafluoroethene), poly(tetrafluoroethene) with 15% aluminium, nylon, cellulose and rubber. The reference spectrum stored for every compound in the library is the average of 15 spectra (5 shots on 3 points of the sample). Being studied 11 organic compounds, the whole spectral library included 165 spectra (15 spectra every sample × 11 samples).

*Step* 4: The linear and rank correlation methods and the method of normalized coordinates were applied using the spectral library. The distribution of correlation coefficients and problem coordinate was studied. The scheme is shown in Fig. 3.

*Step* 5: Statistical criteria must be used in order to quantify the level of significance of the differences in the three methods. A simple Student's *t*-test was applied, thus the probability for each method were calculated.

The methods used to discriminate organic solid materials were methods of correlation and normalized coordinates.

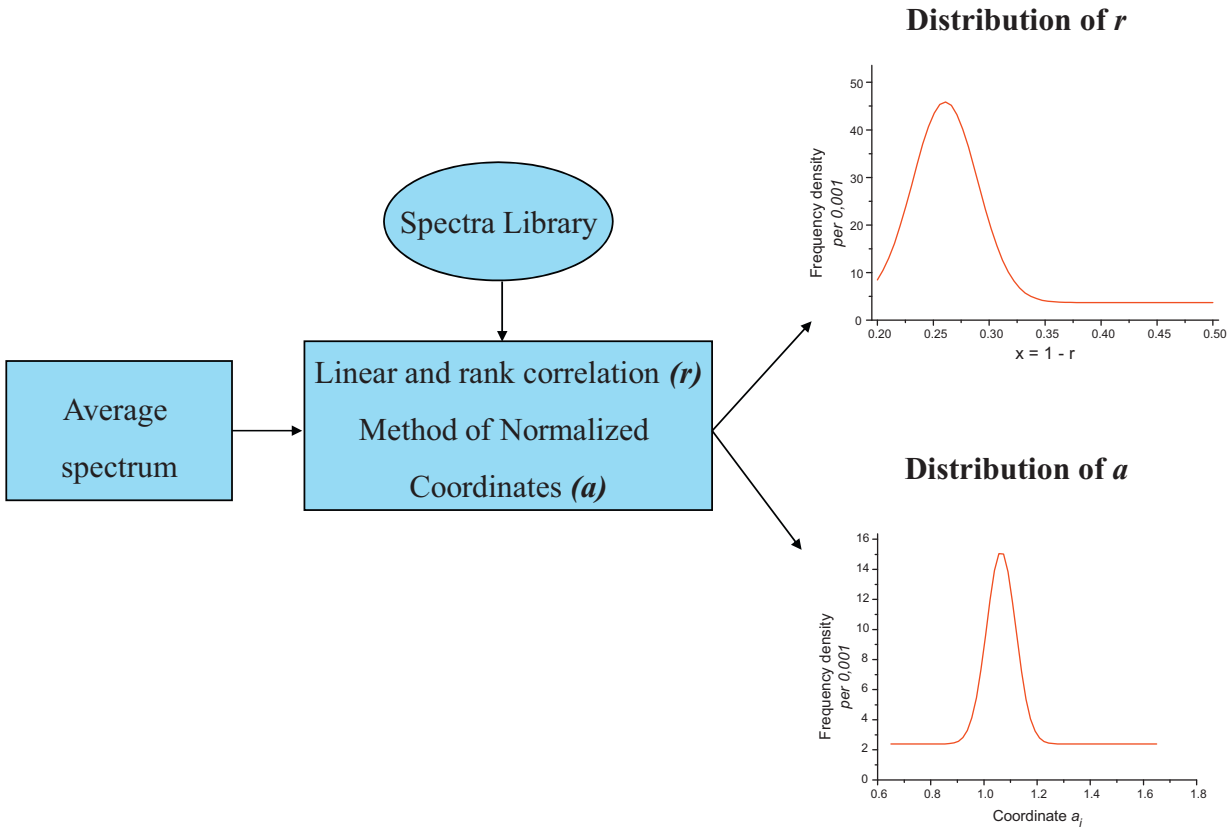


**Fig. 3.** Scheme with the path from multiple single shot spectra to distribution of *r* and *a*.

*2.2.1. Correlation methods*

Linear correlation measures the association between variables with a linear correlation coefficient, r, expressed in the following Eq. (1):

$$r = \frac{\sum_i (x_i - \bar{x})(y_i - \bar{y})}{\sqrt{\sum_i (x_i - \bar{x})^2}\sqrt{\sum_i (y_i - \bar{y})^2}} \quad (1)$$

where $\bar{x}$ is the mean of $x_i$ values, and $\bar{y}$ is the mean of $y_i$ values. The value of $r$ lies between −1 and 1; $r = 1$ corresponds to complete positive correlation when the data points lie on a perfect straight line with positive slope, with $x$ and $y$ increasing together.

The equation for non-parametric correlation is the same as Eq. (1) but now the values of $x$ and $y$ are replaced by their corresponding ranks:

$$r = \frac{\sum_i (R_i - \bar{R})(S_i - \bar{S})}{\sqrt{\sum_i (R_i - \bar{R})^2}\sqrt{\sum_i (S_i - \bar{S})^2}} \quad (2)$$

where $R_i$ is the rank of $x_i$ among the other $x$ values, $S_i$ is the rank of $y_i$ among the other values, $\bar{R}$ and $\bar{S}$ are the average ranks. As before, $x_i$ (or its corresponding rank $R_i$) stands for the intensity of light detected by pixel $i$ in the probe (or current) spectrum, whereas $y_i$ (or its corresponding rank $S_i$) stands for the intensity at the same pixel $i$ of the stored spectra library, which is correlated with the current spectrum. The ranks are numbers 1,2,3,. . .,$N$ where $N$ is a total number of data points (or pixels, 26,904), which replace the true values of $x$ and $y$ in accordance with their magnitudes. For example, the most intense pixel in a spectrum is assigned the number 26,904 in the ICCD detector, the least intense, the number 1, i.e., the higher the intensity, the higher the rank. Hence, the resulting list of numbers is drawn from a perfectly known distribution function, namely uniformly from the integers between 1 and $N$.

A homemade program for correlation analysis written in Visual Basic 6.0 was used. This program has been applied successfully to the identification of different kinds of materials using their LIBS spectra [26,27]. The software offers the following options to an operator: (i) choice of appropriate experimental parameters (integration time, trigger type, spectrometer channel, number of spectra to average, library file); (ii) pre-treatment of the spectrum (reduction in the spectral range, correction for continuous plasma background); and (iii) selection of a correlation method (linear or rank). The computer calculates all mutual correlation coefficients between the current spectrum and all library spectra. The correlation plot corresponding to the maximum correlation coefficient is displayed along with the statistical parameters (correlation coefficients, errors, probabilities) and the name of the compound, which is identified with the highest correlation probability. If desired, the correlation can be repeated with the use of another correlation method. The output data are saved and stored in a computer.

*2.3. Method of normalized coordinates*

This method was described in detail by Ferrero et al. [20]. It is based on the algebraic determination of the problem spectrum coordinates with respect to the library base. The problem of calculating the position of a specific spectrum respect to a library is expressed as the problem of finding the coordinate $a_i$ of a problem vector $p$ in a specific base $\{v\}_i$. It is expressed in Eq. (3).

$$p_j = \sum_{i=1}^{N} a_i v_{ji} \quad (3)$$

where $N$ is the number of vectors in our base (number of spectra in the library), $p_j$ is the coordinate $j$ of the problem vector (problem spectrum at wavelength $j$), $v_{ji}$ is the coordinate $j$ of the component $i$ in our base (spectrum $i$ of the library at wavelength $j$), and $a_i$ is the coordinate $i$ of $p_j$ in the new base. Eq. (3) can be mathematically transformed in Eq. (4).

$$a = (V^T V)^{-1} V^T p \quad (4)$$

where $V^T$ is the transpose of $V$, and $(V^T V)^{-1}$ is the product between this transpose and $V$ which is an invertible square matrix and $p$ is the problem vector. Eq. (4) allows to resolve the problem of calculating the position of spectrum respect to a library. When $a_i$ is equal 1, the spectrum $i$ of the library matches the problem spectrum; and when it is equal 0, the problem spectrum is identified as unknown in the library. An intermediate value may indicate a mixture among the different spectra in the library. Each spectrum was normalized to its maximum intensity value.

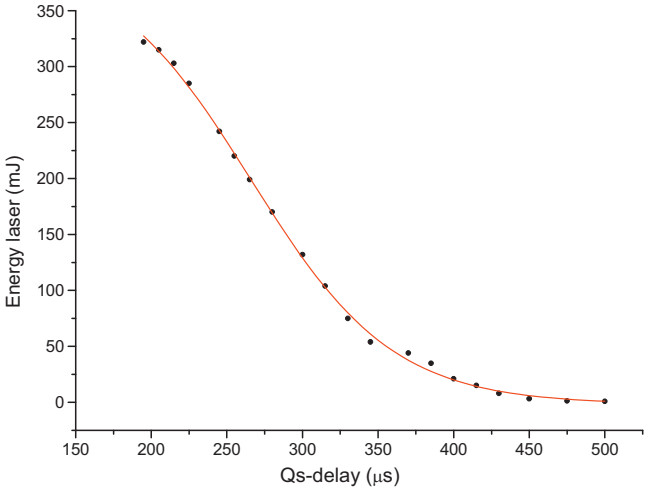


**Fig. 4.** Qs-delay versus pulse laser energy.

## 3. Results and discussion

*3.1. Optimization of LIBS parameters*

The LIBS parameters optimized were: laser energy, delay and integration time depending on the signal-to-noise ratio for the carbon and hydrogen emission lines at 247.9 and 656.3 nm, respectively. These lines were selected because only both emission lines are common for all organic compounds. Also, these emission lines are the most sensitive for both elements and they are free from spectral interference.

The first parameter optimized was the laser pulse energy. A Q-Switched (QS) Nd:YAG laser emitting at 1064 nm was used in this study. In order to optimize the LIBS signal, laser pulse energies were changed by means of the QS trigger delays with respect to the flash-lamp trigger. The laser energy was 322 mJ when the lowest QS-delay was used (195 μs). However, the laser energy was 1 mJ when the QS-delay was the highest. In Fig. 4 it is shown the laser energy variation depending on the QS-delay. The laser energy was studied from 5 to 322 mJ at 1064 nm. In Fig. 5, it is shown the signal-to-noise ratio variation depending on the energy laser for hydrogen emission line at 656.3 nm. The SNR value was maximum at 135 mJ for this line, whereas, the SNR value was maximum at 132 and 330 mJ for carbon line emission. Thus, the optimal energy was selected at 132 mJ because the signal-to-noise ratio was highest for both emission lines. The crater diameter produced by the ablation in these conditions was approximately 0.4 mm; thus, the irradiance was $2.4 \times 10^{10}$ W cm$^{-2}$.

The second parameter optimized was the delay time. Longer delay times are beneficial because, even though total intensity is

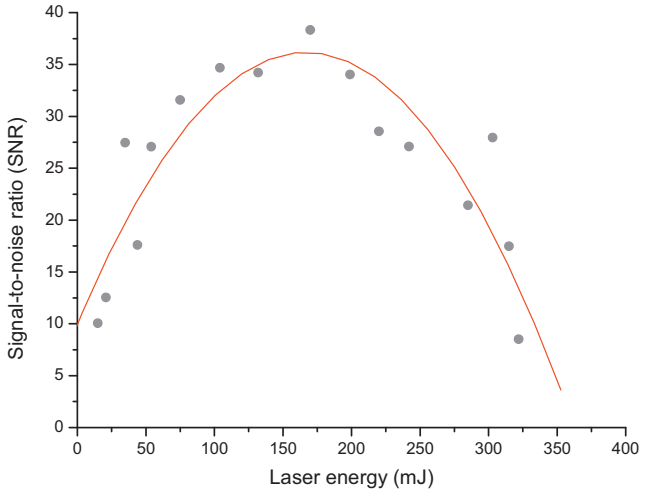


**Fig. 5.** SNR variation depending on the energy laser for hydrogen at 656.3 nm.

decreased, the signal-to-noise ratio is better. Thus, the spectrum that is observed in the first nanoseconds (200 ns) is dominated by continuous, intense, white-light radiation, consequently no discrete lines can be observed. After, discrete spectral lines originating from various species start to become visible. However, if the delay time is too long, the emission lines could disappear.

The delay time was studied on the optimal energy (132 mJ) in the range from 100 to 10,000 ns. The atomic emission signal strength of analyte species in a laser-induced plasma is a function of laser pulse energy and the delay time gate. The signal integration width was fixed at 3000 ns for all measurements in this optimization. The SNR value was studied for delay time optimization and carbon and hydrogen emission lines were analyzed. The SNR variation with the delay time is shown in Fig. 6, for carbon and hydrogen emission lines. Optimal delay time for carbon was approximately 500 ns. The behaviour of intensity and SNR values for hydrogen were similar, although the optimal delay time was approximately 2000 ns. Despite the fact that the hydrogen emission line at 656.3 nm is more intense than carbon emission line at 247.9 nm, the SNR is lower for hydrogen emission line due to high noise in this region of the spectrum. The data did not enable selection of the optimal delay time for both elements because the delay times did not agree; therefore it led to do a statistical treatment of data. The functions of delay time with respect to the incident pulse energies for both emission lines were normalized. The normalized equation for the delay time

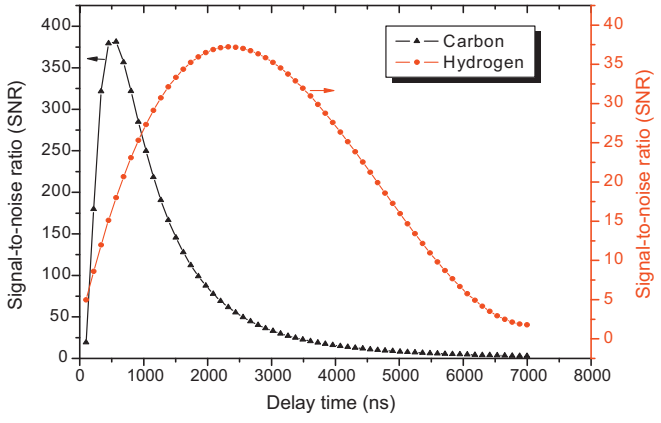


**Fig. 6.** SNR dependence with delay time for carbon and hydrogen emission lines at 249.8 and 656.3 nm, respectively.

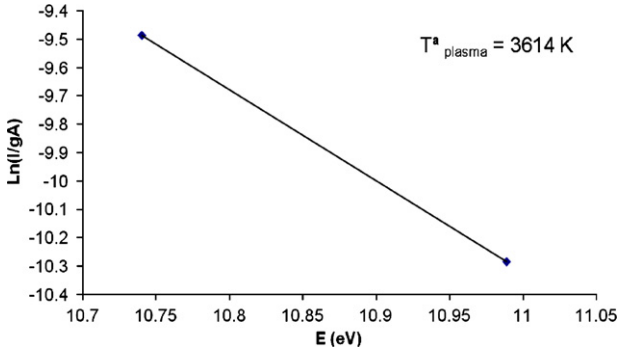


**Fig. 7.** Boltzmann plot of O(*I*) for cellulose.

optimization of the carbon emission line to fit the curve in Fig. 6 is shown in Eq. (5). The values of the coefficients are given in Table 3.

$$y = ax^{(bx^{(-c)})} \tag{5}$$

The normalized equation for the delay time optimization of the hydrogen emission line to fit the curve in Fig. 6 is shown in Eq. (6). The values of the coefficients are given in Table 3.

$$y = a + bx + cx^2 + dx^3 \tag{6}$$

The two normalized Eqs. (5) and (6) were added up to obtain the optimal delay time (630 ns).

Finally, the temporal signal integration was optimized. The SNR was studied from 500 to 25,000 ns. An independent behaviour respect to temporal signal integration was observed for the hydrogen emission line. An optimal integration time was found at 3000 ns for the carbon emission line. Therefore, the optimal value chosen was 3000 ns.

To sum up, the optimal pulse laser energy, delay time and integration time were 132 mJ, 630 ns and 3000 ns, respectively. These optimal parameters LIBS were fixed for the identification of organic solid materials.

### 3.2. Plasma characterization

Plasma temperature was determined using the Boltzmann plot method. Assuming the LTE is established within the plasma, the population in different levels is governed by the Boltzmann distribution. Boltzmann's law relates the LIBS line intensity for the $E_k \rightarrow E_i$ transition of an atomic specie that it is shown in Eq. (7).

$$\ln \frac{I_\lambda^{ki}}{A_{ki} g_k} = -\frac{E_k}{k_B T} + \ln \frac{hcN(T)}{4\pi U(T)} \tag{7}$$

where $I$ is the intensity of each spectral line, $A_{ki}$ and $g_k$ are the transition probability and the statistic weight of the upper energy level $E_k$, $k_B$ and $h$ are the Boltzmann and Planck constants, $c$ is the velocity of the light, and $U(T)$ and $N(T)$ are partition function and total density of emitting species, respectively. This relation leads to a linear plot against $E_k$ if several transitions of the same species are considered. The temperature of this species can be deduced from the slope of such a plot. The graph $\ln I/(gA)$ vs. $E$ is plotted for O($I$) emission lines at 777.4 nm and 844.6 nm as it is shown in Fig. 7 and the corresponding plasma temperature estimated from such plot is 3614 K for cellulose. The spectral lines for O($I$) are specified in Table 1 from the LIBS spectra for intensity measurement.

In a plasma source the line-width is due to Stark broadening, which results from collisions of charged species [28], whereas pressure and Doppler broadenings are quite small [29]. The electron density is calculated from the Stark broadening of O($I$) at 777.4 nm for cellulose, whose Lorentzian line shape function is shown in

**Table 1**
Spectroscopic data $g$, $A$, and $E$ for upper energy levels of O($I$). (NIST atomic spectroscopy databases, http://www.nist.gov/pml/data/atomspec.cfm.)

| Wavelength (nm) | | $g, A$ ($s^{-1}$) | $E_i$ (eV) | | $E_k$ (eV) | Transitions | |
|---|---|---|---|---|---|---|---|
| O($I$) | 777.19 | $2.58 \times 10^{08}$ | 9.14 | – | 10.74 | 2s22p3(4S°)3s– | 2s22p3(4S°)3p |
| O($I$) | 777.42 | $1.84 \times 10^{08}$ | 9.14 | – | 10.74 | 2s22p3(4S°)3s– | 2s22p3(4S°)3p |
| O($I$) | 777.54 | $1.11 \times 10^{08}$ | 9.14 | – | 10.74 | 2s22p3(4S°)3s– | 2s22p3(4S°)3p |
| O($I$) | 844.62 | $3.22 \times 10^{07}$ | 9.52 | – | 10.98 | 2s22p3(4S°)3s– | 2s22p3(4S°)3p |
| O($I$) | 844.63 | $1.61 \times 10^{08}$ | 9.52 | – | 10.98 | 2s22p3(4S°)3s– | 2s22p3(4S°)3p |
| O($I$) | 844.67 | $9.66 \times 10^{07}$ | 9.52 | – | 10.98 | 2s22p3(4S°)3s– | 2s22p3(4S°)3p |

**Table 2**
Emission lines and bands.

| Element | Wavelength (nm) |
|---|---|
| Carbon | 247.9 (w,I) |
| CN band | 388 (s) |
| Hydrogen | 656.3 (s, $H_\alpha$) |
| Nitrogen | 500 (s,II); 746.8 (w,I); 868.3 (w, I) |
| Oxygen | 777.4 (w, triplet); 844.6 (w,I) |
| Sodium | 588–589 (s, doublet) |
| Swan band (C2) | 467 (m,II); 517 (s,II); 550 (m,II) |

w: weak; m: medium; s: strong.

Fig. 8. The observed line-width, FWHM ($\Delta\lambda_{observed}$), have been corrected by subtracting the instrumental width ($\Delta\lambda_{instrument}$) whose value is 0.01 nm for the spectrometer. The corrected value was 0.466. The electron density ($N_e$), related to the Full width at half maximum (FWHM) $\Delta\lambda$ of the stark broadened line is shown in Eq. (8).

$$N_e = \frac{\Delta\lambda \times 10^{16}}{2w}[\mathrm{cm}^{-3}] \tag{8}$$

where $\Delta\lambda$ is FWHM and w is the electron impact parameter which can be obtained corresponding to different plasma temperature [30]. The electron density calculated using (8) was $1.17 \times 10^{18}$ cm$^{-3}$. The McWhirter criterion, which provides the lowest value of the electron density necessary for the plasma to reach the LTE condition of local thermal equilibrium requires verify Eq. (9).

$$N_e \geq 1.6 \times 10^{12} T^{1/2} \Delta E^3 \tag{9}$$

where $N_e$ (cm$^{-3}$) is the electron density, $T$ (K) is the plasma temperature, and $\Delta E$ (eV) is the largest energy transition. According to this criterion, if the largest energy ($\Delta E$) is 1.6 eV and plasma temperature is 3614 K, Eq. (9) results in a minimal electron density value of $N_e = 3.94 \times 10^{14}$ cm$^{-3}$. The electron density obtained from Eq. (8) is greater than its respective lower limit given by Eq. (9), so the condition for LTE is fulfilled at optimal parameters. The electron density as a function of delay at optimal energy is shown in Fig. 9. The plasma emission spectra recorded as a function of the detection delay, it allowed to study the temporal evolution of the electron density in the plasma during its expansion and decay.

Also, the plasma must be optically thin. The intensity ratio of two lines of the same species of ionization stage $Z$ can be expressed as

$$\frac{I_1}{I_2} = \left(\frac{\lambda_{nm,Z}}{\lambda_{ki,Z}}\right)\left(\frac{A_{ki,Z}}{A_{nm,Z}}\right)\left(\frac{g_{k,Z}}{g_{n,Z}}\right)\exp\left(-\frac{E_{k,Z} - E_{n,Z}}{k_B T}\right) \tag{10}$$

where $I_1$ is the line intensity from the $k$–$i$ transition and $I_2$ is that from the $n$–$m$ transition. If we consider two emission lines having the same upper level or as close as possible, the temperature effect of the Boltzmann factor on the reproducibility of the line intensity ratio is minimized and at the same time the consideration of the efficiency factor of the collecting system is avoided. By matching this ratio with the measured values at different delay times, one finds out the time window where the plasma is optically thin. The time window where the plasma is optically thin and is also in LTE is inferred from the temporal evolution of the intensity ratio of two Ca lines, 393.3 and 396.8 nm, which have upper levels having very close energy. This element was present in all samples, it should be an impurity in the manufacturing process, although it is useful for this purpose. Fig. 10 shows the temporal evolution of the intensities of these lines and the intensity ratio between them. The intensity ratio for this couple of lines was calculated using Eq. (10). Comparing the experimental data of the intensity ratio with the theoretical one, the optically thin plasma was verified.

### 3.3. Correlation methods and method of normalized coordinates

This study focuses on the identification of 11 organic solid materials using linear and rank correlation, and the method of normalized coordinates. The three statistical methods were applied using the spectral library. This library of 165 averaged spectra is shown in Fig. 11. In these spectra, the C2 Swan system and the CN band, as well as the carbon, hydrogen, oxygen and nitrogen,

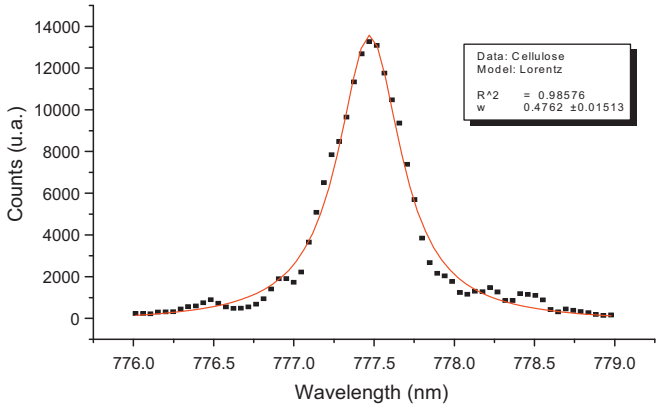


**Fig. 8.** Lorentzian profile of O($I$) of cellulose.

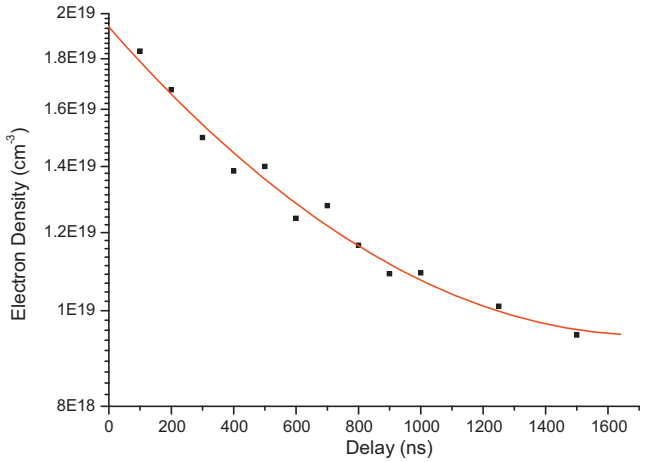


**Fig. 9.** Electron density in the plasma induced on the cellulose at optimal conditions.

**Table 3**
Values of the coefficients of equations.

| | *a* | *b* | *c* | *d* |
|---|---|---|---|---|
| Eq. (5) | 5.166E − 28 ± 6.62E − 31 | 27.58861 ± 0.5322 | 0.16157 ± 0.00027 | |
| Eq. (6) | 0.04476 ± 2.5102E − 16 | 0.00091 ± 3.0443E − 19 | $-2.5948 \times 10^{-7} \pm 9.9319 \times 10^{-23}$ | $1.8411 \times 10^{-11} \pm 9.1986 \times 10^{-27}$ |

emission lines can be detected, which are necessary parameters to identify organic solid materials. Oxygen, nitrogen and hydrogen emission lines and a number of molecular bands are used for this task. The analysis of molecular bands [31,32] is focused on the detection of CN molecular violet bands at 386.17 nm, 387.14 nm and 388.34 nm, and C2 carbon Swan bands at 516.52 nm. The intensity of the Swan system is proportional to the concentration of the carbon dimmer in the excited state, while the CN bands emission could also be due to CN generation in the ambient air. Hence, only the measurement of the C2 bands is reliable for analysis in the open atmosphere. The emission lines selected were: carbon at 247.9 nm, alpha-hydrogen at 656.3 nm, nitrogen at 746.8 nm, 868.3 nm and oxygen at 777.4 nm, 844.6 nm. The emission lines and bands are indicated in Table 2. All organic compounds LIBS spectra are like among them. These organic compounds are almost entirely atomized when exposed to intense laser radiation sufficient for breakdown. This implies that limitations exist in application of LIBS for discriminated organic solid materials because of the loss of molecular information in the plasma. However intensity relative differences are observed, due to stoichiometric differences. Also, the large amount of spectroscopic data used all at once in the correlation procedure, allows original information about the sample nature to be obtained.

The reference spectrum of each sample was correlated against the library. Linear and rank correlation coefficients and problem coordinate *a* are calculated for each individual spectrum versus the library. Finally, the maximum correlation coefficient and the sample associated with the highest correlation coefficient are obtained. The highest correlation coefficient indicated a similarity of a tested spectrum to one from the library. The difference between this and other correlation coefficients indicates spectral and, hence, compositional differences.

Besides the similarities among samples determined by the statistical methods, statistical criteria must be used in order to quantify the level of significance of the differences in three methods. A simple Student's *t*-test was applied to choose the probability of similarities among samples. The distribution of correlation coefficients and problem coordinate was studied. The normality of the distribution is shown in Fig. 12. A simple analysis by Student's *t*-test was applied. This is a hypothesis test for two population means to determine whether they are significantly different when the distri-

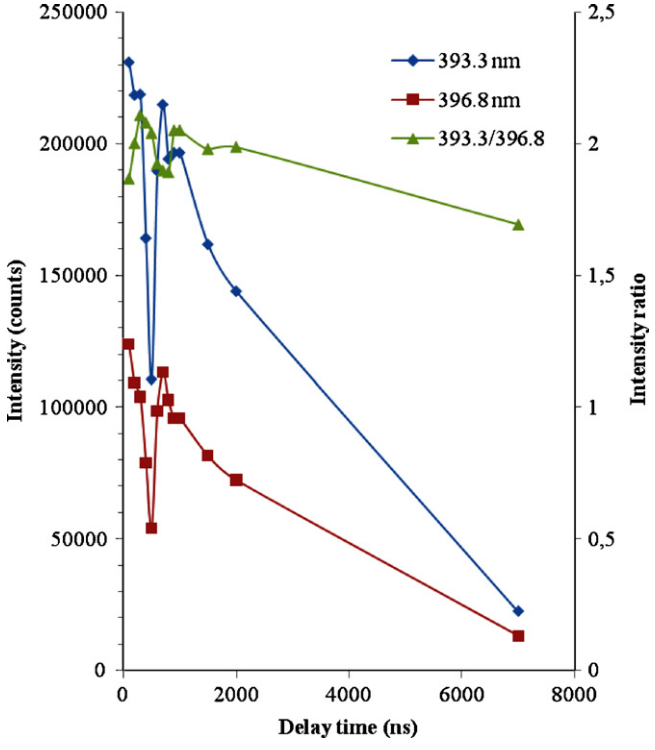


**Fig. 10.** Temporal evolution of intensities of two Ca lines 393.3 and 396.8 nm and their intensity ratio.

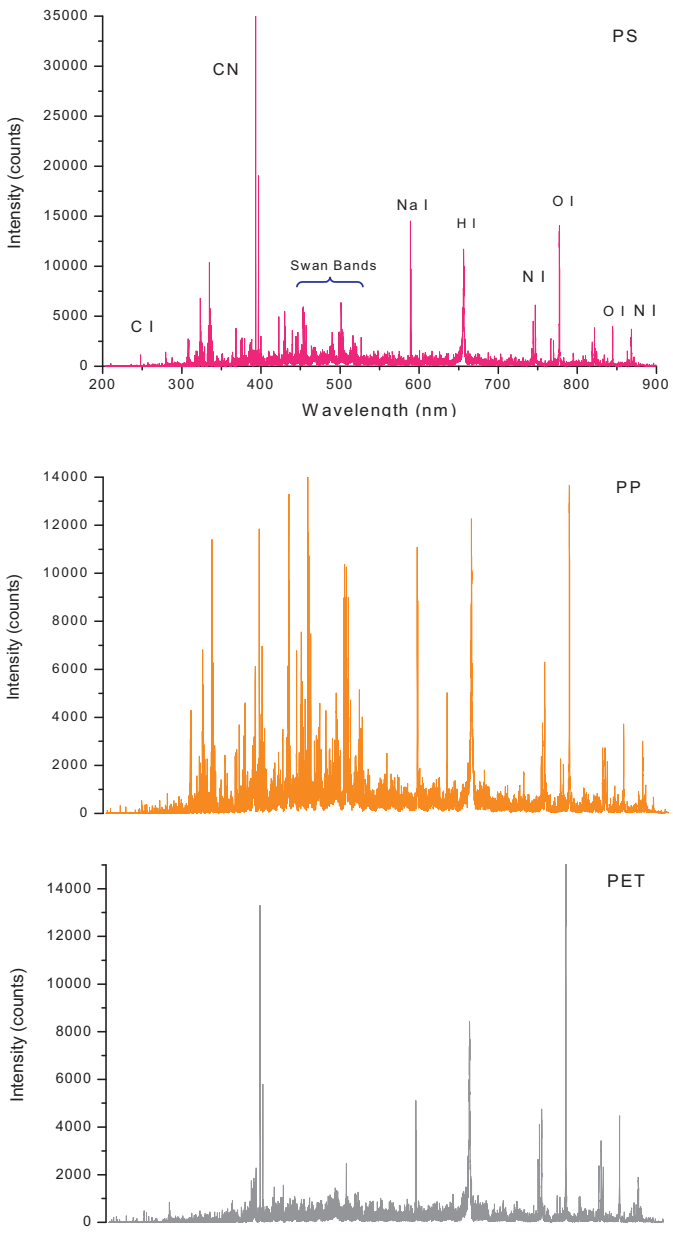


**Fig. 11.** Spectra library of organic solid materials.

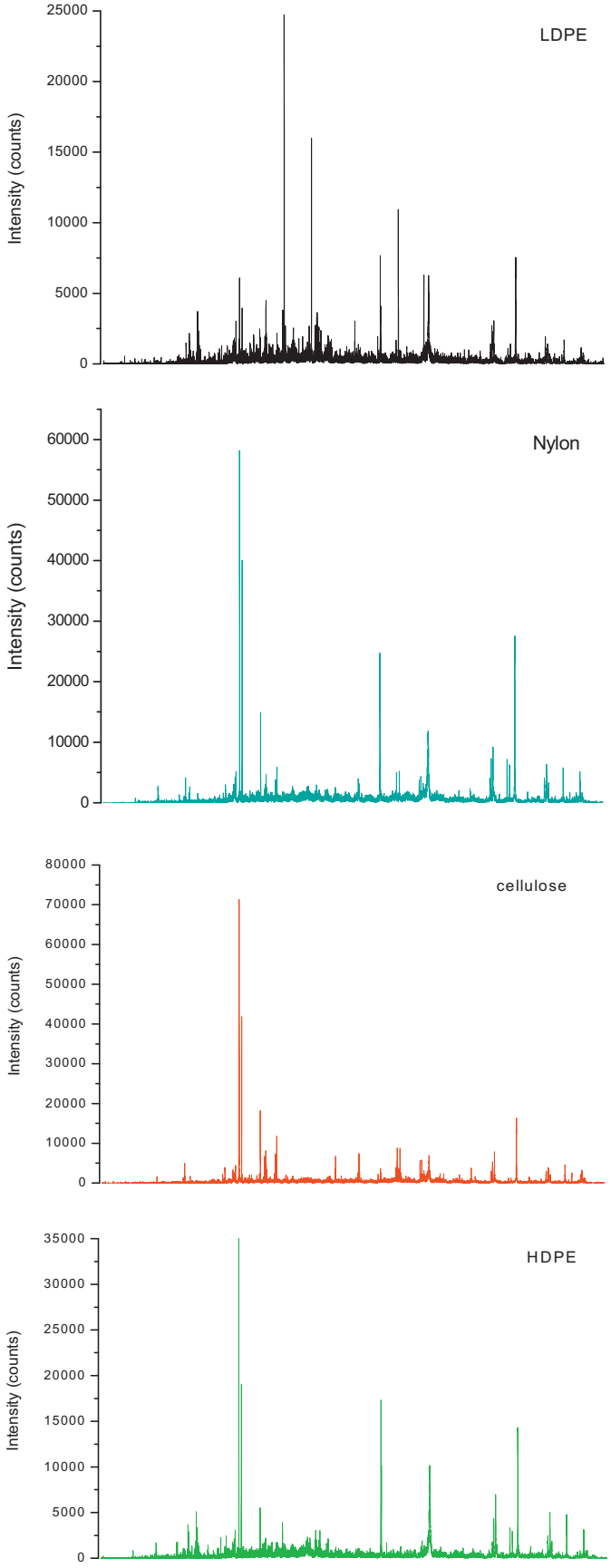


**Fig. 11.** (*Continued*)

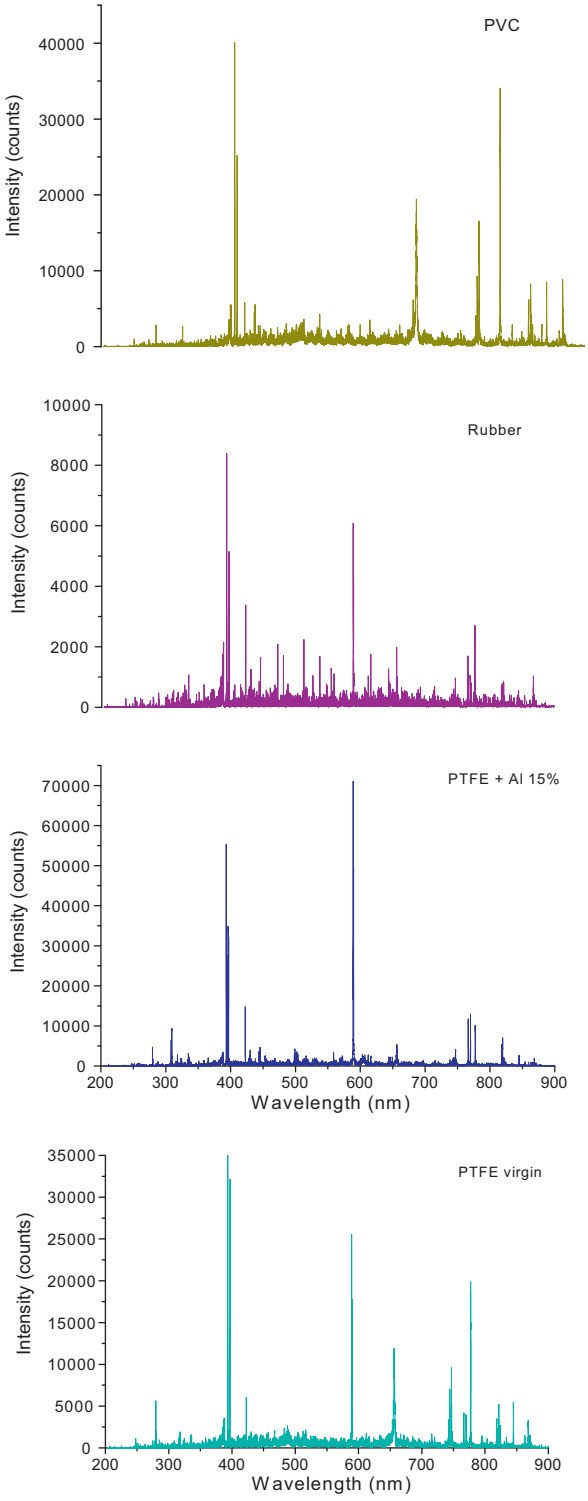


**Fig. 11.** (*Continued*)

butions of the populations are close to normal. The normality of the distribution of the correlation coefficients is proven using normality plots ($Q$–$Q$ plots) for linear and rank correlation and normalized coordinates; the results showed normality for these distributions. Using the $t$-test, the null hypothesis is that the difference between two population means of correlation coefficients is equal to zero and it is tested against an alternative hypothesis in which they are not. The $p$-values are used in hypothesis tests and represent the probability of making a Type 1 error, which is rejecting the null

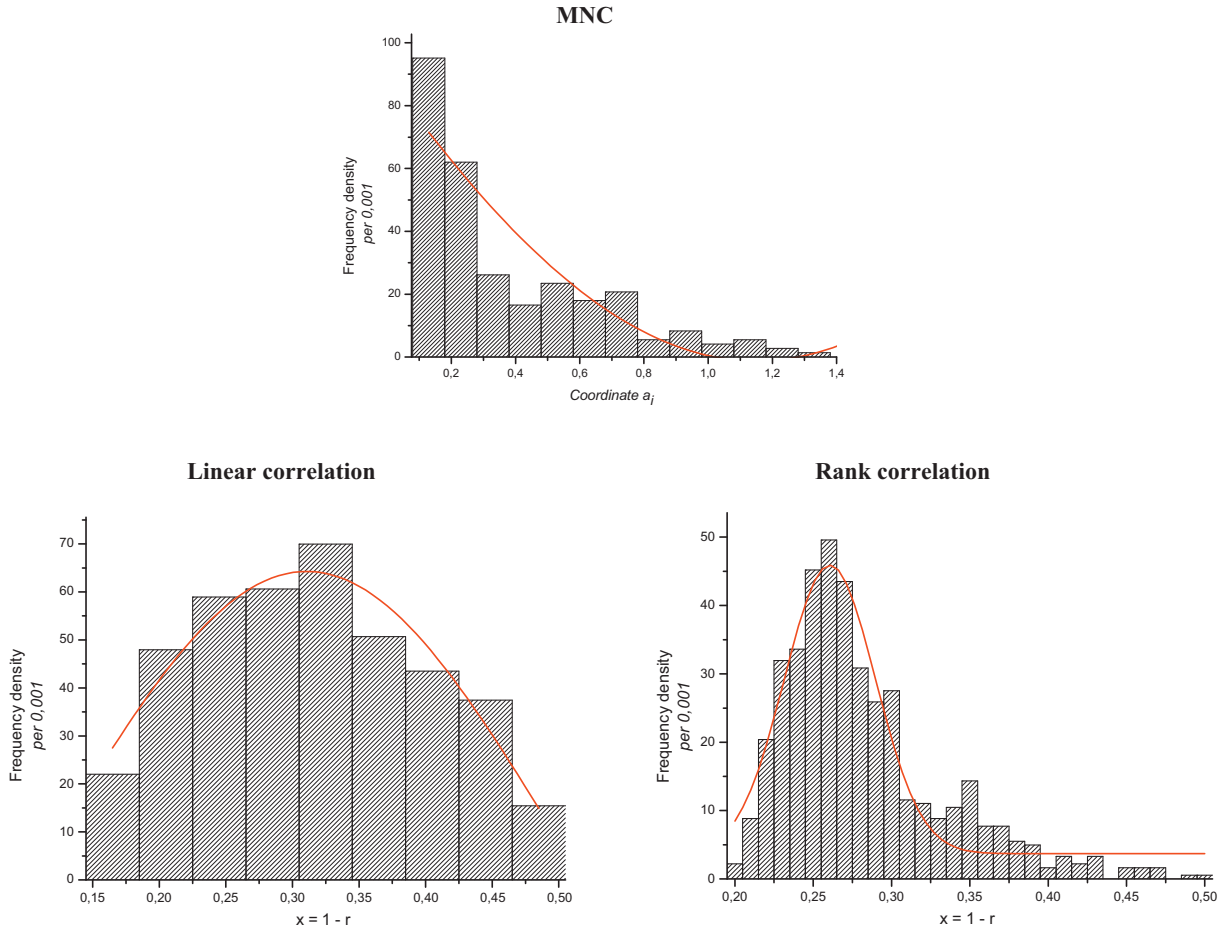


**Fig. 12.** Normal distribution of correlation coefficients and problem coordinate.

**Table 4**
Detected similarities among samples using *p*-values obtained by test *t*-Student ($p > 0.05$).

| | M1 | M2 | M3 | M4 | M5 | M6 | M7 | M8 | M9 | M10 | M11 |
|---|---|---|---|---|---|---|---|---|---|---|---|
| Linear | | | | M2 | | M3<br>M8<br>M11 | | M3<br>M9 | | | M6<br>M10 |
| Rank | M2 | | | | | M7<br>M10 | M10<br>M11 | M3 | | | M7 |
| MNC | M2–M11 | M4–M11 | | | M9 | M1–M5<br>M7–M11 | M9 | M3<br>M9 | | M9<br>M11 | M9 |

M1: PTFE + 15%Al, M2: PTFE virgin, M3: PVC, M4: rubber, M5: cellulose, M6: HDPE, M7: LDPE, M8: nylon, M9: PET, M10: PP and M11: PS.

hypothesis when it is true. If the test's *p*-value is less than the chosen significance level ($p = 0.05$ to give a 95% confidence level) the null hypothesis is rejected and it is concluded that the samples are different. Otherwise, the results suggest there is no significant difference between the two populations, in other words, there is no significant difference between the two samples. The 11 samples provide 55 possible pair of comparisons. Based on the *p*-values, the results of similarity among samples are shown in Table 4. This table shows that the correlation coefficients obtained by linear correlation indicate similarities for M4 and M2, M6 and M3, M8, M11, M8 and M3, M9, M10 and M11, providing 87,3% correct identification at a 95% confidence level. However, rank correlation indicated similarity among samples M1 and M2, M6 and M7, M10, M11, M7 and M10, M11, M8 and M3, which is incorrect. Rank correlation provided an overall 87.3% correct identification at a 95% confidence level. The MNC indicated similarities among samples M1 and all samples, M2 and all samples except M3. Moreover, the following similarities were chosen among M5 and M9, M6 and all samples except M1 and M2. Among M7 and M9, M8 and M3, M9, M10 and M9, M11 and finally M11 and M9, which are not true, yielding 40% correct identifications at a 95% confidence level in both methods.

## 4. Conclusions

In this work parameters LIBS has been optimized for discriminating organic solid materials. Moreover, the plasma characterization was done and following the LTE conditions, the McWhirter criteria are fulfilled for optimal conditions. Also, the optically thin plasma was verified. The present study demonstrates that LIBS is capable of characterizing organic solid materials with similar chemical composition. It is possible to discriminate between LDPE and HDPE both with the same chemical composition. Moreover, LIBS has the potential to discriminate one from the other by means of the methods of linear and rank correlation

and method of normalized coordinates. Linear and rank correlation provides 87.3% correct identification at a 95% confidence level. However, the MNC provides only 40% correct identification at a 95% confidence level. It is concluded that linear and rank correlation provides better results than the MNC.

## Acknowledgements

The authors thank to Dr.I. Gornushkin and Dr. N. Omenetto for their help. This work was supported by the Environment Ministry of the Spanish National Government through project #344/2007/3-2.7. We would also like to give special thanks to the Department of Science, Technology and University of the Aragon Regional Government and the ESF for financing our research group E75 and proposal # PI 045/09 and to the University of Zaragoza, proposal # UZ2009-CIE-01.

## References

[1] W.B. Lee, J. Wu, Y.I. Lee, J. Sneddon, Recent applications of laserinduced breakdown spectrometry: a review of material approaches, Appl. Spectrosc. Rev. 39 (2004) 27–97.
[2] E. Tognoni, V. Palleschi, M. Corsi, G. Cristoforetti, Quantitative micro-analysis by laser-induced breakdown spectroscopy: a review of the experimental approaches, Spectrochim. Acta Part B 57 (2002) 1115–1130.
[3] J. Anzano, R.J. Lasheras, Strategies for the identification of urinary calculus by laser induced breakdown spectroscopy, Talanta 79 (2009) 352–360.
[4] S. Rai, A.K. Rai, S.N. Thakur, Identification of nitro-compounds with LIBS, Appl. Phys. B 91 (2008) 645–650.
[5] F. Yueh, J.P. Singh, H. Zhang, Encyclopedia of Analytical Chemistry, Wiley, 2000.
[6] N. Carmona, M. Oujja, E. Rebollar, H. Römich, M. Castillejo, Analysis of corroded glasses by laser induced breakdown spectroscopy, Spectrochim. Acta Part B 60 (2005) 1155–1162.
[7] E.C. Ferreira, J.M. Anzano, D.M.B.P. Milori, E.J. Ferreira, R.J. Lasheras, B. Bonilla, B. Montull-Ibor, J. Casas, L. Martin Neto, Multiple response optimization of laser-induced breakdown spectroscopy parameters for multi-element analysis of soil samples, Appl. Spectrosc. 63 (2009) 1081–1088.
[8] L.C. Nunes, Gilmare Antônia da Silvac, L.C. Trevizanb, D.S. Júniord, R.J. Poppie, F.J. Krug, Simultaneous optimization by neuro-genetic approach for analysis of plant materials by laser induced breakdown spectroscopy, Spectrochim. Acta Part B 64 (2009) 565–572.
[9] J.W. Batista, L.C. Trevizan, L.C. Nunes, I. Aparecida, D. Santos Jr., F.J. Krug, Comparison of univariate and multivariate calibration for the determination of micronutrients in pellets of plant materials by laser induced breakdown spectrometry, Spectrochim. Acta Part B 65 (2010) 66–74.
[10] I.B. Gornushkin, B.W. Smith, H. Nasajpour, J.D. Winefordner, Identification of solid materials by correlation analysis using a microscopic laser-induced plasma spectrometer, Anal. Chem. 71 (1999) 5157–5164.
[11] J.M. Anzano, I.B. Gornushkin, B.W. Smith, J.D. Winefordner, Laser-induced plasma spectroscopy for plastic identification, Polym. Eng. Sci. 40 (2000) 2423–2429.
[12] J. Anzano, M. Casanova, M.S. Bermúdez, R.J. Lasheras, Rapid characterization of plastics using laser-induced plasma spectroscopy (LIPS), Polym. Test. 25 (2006) 623–627.
[13] M. Tran, Q. Sun, B.W. Smith, J.D. Winefordner, Determination of C:H:O:N ratios in solid organic compounds by laser-induced plasma spectroscopy, J. Anal. At. Spectrom. 16 (2001) 628–632.
[14] J. Anzano, R.J. Lasheras, B. Bonilla, J. Casas, Classification of polymers by determining of C-1:C-2:CN: H:N:O ratios by laser-induced plasma spectroscopy (LIPS), Polym. Test. 27 (2008) 705–710.
[15] B. Bousquet, J.B. Sirven, L. Canioni, Towards quantitative laser-induced breakdown spectroscopy analysis of soil samples, Spectrochim. Acta Part B 62 (2007) 1582–1589.
[16] C. Bohling, K. Hohmann, D. Scheel, C. Bauer, W. Schippers, J. Burgmeier, U. Willer, G. Holl, W. Schade, All-fiber-coupled laser-induced breakdown spectroscopy sensor for hazardous materials analysis, Spectrochim. Acta Part B 62 (2007) 1519–1527.
[17] S. Duchene, V. Detalle, R. Bruder, J.B. Sirven, Current chemometrics and laser induced breakdown spectroscopy (LIBS) analyses for identification of wall paintings pigments, Anal. Chem. 6 (2010) 60–65.
[18] C.A. Munson, F.C. De Lucia Jr., T. Piehler, K.L. McNesby, A.W. Miziolek, Investigation of statistics strategies for improving the discriminating power of laser-induced breakdown spectroscopy for chemical and biological warfare agent simulants, Spectrochim. Acta Part B 60 (2005) 1217–1224.
[19] J.B. Sirven, B. Bousquet, L. Canioni, L. Sarger, Qualitative and quantitative investigation of chromium-polluted soils by laser-induced breakdown spectroscopy combined with neural networks analysis, Anal. Chem. 78 (2006) 1462–1469.
[20] A. Ferrero, P. Lucena, R.G. Herrera, A. Doña, R. Fernández-Reyes, J.J. Laserna, Libraries for spectrum identification: method of normalized coordinates versus linear correlation, Spectrochim. Acta Part B 63 (2008) 383–388.
[21] J.B. Sirven, B. Bousquet, L. Canioni, L. Sarger, S. Tellier, M. Potin-Gautier, I. Le Hecho, Qualitative and quantitative investigation of chromium-polluted soils by laser-induced breakdown spectroscopy combined with neural networks analysis, Anal. Bioanal. Chem. 385 (2006) 256–262.
[22] S.R. Goode, S.L. Morgan, R. Hoskins, A. Oxsher, Identifying alloys by laser-induced breakdown spectroscopy with a time-resolved high resolution echelle spectrometer, J. Anal. At. Spectrom. 15 (2000) 1133–1138.
[23] V. Lazic, F. Colao, R. Fantoni, V. Spizzicchino, Recognition of archeological materials underwater by laser induced breakdown spectroscopy, Spectrochim. Acta Part B 60 (2005) 1014–1024.
[24] E.M. Rodriguez-Celis, I.B. Gornushkin, U.M. Heitmann, J.R. Almirall, B.W. Smith, J.D. Winefordner, N. Omenetto, Laser induced breakdown spectroscopy as a tool for discrimination of glass for forensic applications, Anal. Bioanal. Chem. 391 (2008) 1961–1968.
[25] A. Sarkar, S.K. Aggarwal, D. Alamelu, Laser induced breakdown spectroscopy for rapid identification of different types of paper for forensic application, Anal. Methods 2 (2010) 32–36.
[26] I.B. Gornushkin, A. Ruiz-Medina, J.M. Anzano, B.W. Smith, J.D. Winefordner, Identification of particulate materials by correlation analysis using a microscopic laser induced breakdown spectrometer, J. Anal. At. Spectrom. 15 (2000) 581–586.
[27] J.M. Anzano, M. Villoria, I.B. Gornushkin, B.W. Smith, J.D. Winefordner, Laser-induced plasma spectroscopy for characterization of archaeological material, Can. J. Anal. Sci. Spectrosc. 47 (2002) 134–140.
[28] D.K. Rai, S.N. Thakur, Atomic Spectra Structure and Modern Spectroscopy, Vaivaswat, Varanasi, 2005.
[29] N.M. Shaikh, B. Rashid, S. Hafeez, Y. Jamil, M.A. Baig, Measurement of electron density and temperature of a laser-induced zinc plasma, J. Phys. D: Appl. Phys. 39 (2006) 1384–1391.
[30] H.R. Griem, Plasma Spectroscopy, McGraw-Hill, New York, 1964.
[31] L. St-Onge, R. Sing, S. Bé chard, M. Sabsabi, Carbon emissions following 1.064 μm laser ablation of graphite and organic samples in ambient air, Appl. Phys. 69 (1999) 913–916.
[32] A. Portnov, S. Rosenwaks, I. Bar, Emission following laser-induced breakdown spectroscopy of organic compounds in ambient air, Appl. Opt. 42 (2003) 2835–2842.